ISSN 0965-5441, Petroleum Chemistry, 2023, Vol. 63, No. 7, pp. 790–797. © Pleiades Publishing, Ltd., 2023.
ISSN 0965-5441, Petroleum Chemistry, 2023. © Pleiades Publishing, Ltd., 2023.
Russian Text © The Author(s), 2023, published in Sovremennye Molekulyarnye Sita. Advanced Molecular Sieves, 2023, Vol. 5, No. 2.

Adsorption Capacity and Biological Activity of Synthetic Zeolites

N. Yu. Ul'yanova[a,*], E. Yu. Brazovskaya[a], O. Yu. Golubeva[a], and O. V. Shamova[b]

[a] *Grebenshchikov Institute of Silicate Chemistry, Russian Academy of Sciences, St. Petersburg, 199034 Russia*
[b] *Institute of Experimental Medicine, St. Petersburg, 197376 Russia*
**e-mail: TernovayaNatali@gmail.com*

Received June 27, 2023; revised July 25, 2023; accepted July 27, 2023

Abstract—The study investigates the physicochemical, porous/textural, and adsorptive properties, as well as the biological activity of BEA, RHO, PAU, and FAU(Y) synthetic zeolites. The adsorption capacity of the zeolites for oxytocin, lysozyme, and albumin—markers of low- and medium-molecular-weight pathological proteins—was measured. The concentration-dependent effects of the zeolites on the viability of human endothelial cells (Ea.hy926) were evaluated. At concentrations of 2.5 to 10 mg/mL, the Y zeolite was found to exhibit no pronounced cytotoxicity. In the presence of the BEA, the cell viability decreased to 80% even at 2.5 mg/mL. The RHO and PAU were shown to have the highest cytotoxicity and significantly inhibit the growth of human cells (down to 23–35%). The study demonstrated that only BEA and Y, among the synthetic zeolites tested, have good biomedical potential due to their high adsorption capacity, low hemolytic activity, and low cytotoxicity.

Keywords: zeolites, adsorption, proteins, hemolytic activity, cytotoxicity

DOI: 10.1134/S096554412305002X

Researchers have recently paid increasing attention to developing biocompatible sorbents for selective adsorption of toxins (e.g., prions, proinflammatory cytokines, viral and bacterial products, etc.) that accumulate in the body in cancer, immune, infectious, and other diseases [1]. For example, intoxication has been found to be mainly caused by accumulation of low-molecular-weight toxins [2]. The choice of sorbent is of particular importance because the properties of the material have a major effect on its selectivity towards specific toxins and on the therapeutic benefits in general [3]. In the cases of acute poisoning with low-molecular-weight toxins, microporous sorbents have proven the most effective. On the other hand, diseases accompanied by accumulation of high-molecular-weight toxins require meso- and macroporous materials to be used.

Thus, selective adsorbability for molecules with specific sizes is a critical property of a medical sorbent. Zeolites possess this sort of selectivity due to their porosity. Zeolites have a unique porous structure: their three-dimensional framework is riddled with pores and channels of specific sizes, which form micro- and mesoporous space.

There are a number of promising medical applications for zeolites, including development of precise drug delivery systems with prolonged release, enterosorption, hemosorption, and application sorption [4]. Most published research in this field has investigated natural zeolites (e.g., clinoptilolite and chabazite) [5–7]. Unfortunately, medical uses of zeolites have remained very limited. This is mainly because of the pronounced hemolytic activity and cytotoxicity of natural zeolites such as chabazite and clinoptilolite, the extent of which likely depends on the presence of impurity phases [8]. For example, a mineral phase in rocks might contain smectites, quartz, chalcedony, and potassium feldspars, in addition to zeolites [9]. It would be has been reasonable to assume that the zeolite toxicity challenge can be overcome by using synthetic zeolites due to their phase purity [10]. However, available research on the applicability of synthetic zeolites as medical sorbents lacks reports on their effects on human cells.

Therefore, it is of undoubted importance to investigate—in terms of adsorption activity for specific bioactive groups and toxicity—various synthetic

Table 1. Zeolite synthesis conditions

Sample	Formulation	Template	Aging time, h	Synthesis conditions	
				temperature, °C	time, h
BEA	Na_7 [$Al_7Si_{57}O_{128}$]	TEAOH[a]	2	140	72
RHO	$(Na,Cs)_{12}$ $(H_2O)_{44}$ [$Al_{12}Si_{36}O_{96}$]	18-C-6[b]	24	120	192
PAU	$(K_2,Na_2)_{76}$ $(H_2O)_{700}$ [$Al_{152}Si_{520}O_{1344}$]	TEAOH	48	120	384
Y	Na_{58} $(H_2O)_{240}$ [$Al_{58}Si_{134}O_{384}$]	–	0	75	20

[a] TEAOH is tetraethylammonium hydroxide.
[b] 18-C-6 is crown ether.

zeolites differing in grain size, porosity, and chemical composition.

Synthesis of zeolites with adjustable properties makes it possible to examine the effects of zeolite type and chemical composition on their adsorption capacity and bioactivity. This being so, the purpose of the present study was to synthesize BEA, RHO, PAU, and FAU(Y) zeolites and to characterize their adsorption activity for proteins, hemolytic activity, and cytotoxicity, as well as to assess their applicability as safe medical sorbents.

EXPERIMENTAL

Zeolites were synthesized under hydrothermal conditions in accordance with the procedures described in [11, 12]. The gel preparation and synthesis conditions are specified in Table 1. The gels crystallized in steel autoclaves (with a filling factor of 0.7). The synthesized zeolites were converted to hydrogen forms by substituting alkaline cations in accordance with the procedure described in [12], where the decationation steps included calcination at 400–550°C to remove the organic template from the zeolite and, thus, empty the porous space.

XRD examination was performed on a Rigaku SmartLab 3 powder diffractometer in CuK_α radiation at 40 kV/40 mA. This diffractometer, equipped with a semiconductor detector capable of 0D (point) and 1D (linear) measurements, was operated in a θ–θ geometry in a 2θ range of 5°–55° with a step of 0.01°. The ICDD-2006 international database was used for phase identification.

The morphology of the synthesized samples was examined by scanning electron microscopy (SEM) on a VEGA3 TESCAN instrument. The samples were prepared using carbon film deposition.

The specific surface area and pore volume were measured by low-temperature nitrogen adsorption on a Quantachrome NOVA 1200e instrument using NOVAWin software. The Langmuir model and the Halsey *t*-method were used to evaluate the specific surface area and external surface area of the zeolites, respectively.

The cation-exchange capacity (CEC) of the samples was determined by ion exchange with hexamine cobalt $[Co(NH_3)_6]^{3+}$. Samples weighing 250 mg were dispersed in 15 mL of a 0.05 M hexamine cobalt chloride solution. The suspension was stirred for 2 h and centrifuged. The CEC was evaluated as the difference between the stock solution and zeolite-containing equilibrium solutions. The concentrations were determined by UV absorption spectroscopy using a LEKISS2109UV UV spectrophotometer based on the absorption band with a maximum at λ_{max} = 473 nm. For each sample, the CEC was determined as the arithmetic mean of five independent measurements.

To characterize the adsorption activity of the synthetic zeolites, we used a number of substances that simulated pathological proteins (specifically, oxytocin, albumin, and lysozyme). These substances served as markers for low-molecular-weight and medium-molecular-weight toxic proteins. The main characteristics of the marker proteins are presented in Table 2. Oxytocin (10 IU/mL, BioFarmGarant, Russia) was used as a marker for low-molecular-weight toxins, and lysozyme (chicken egg protein, Roche) and albumin (lyophilized bovine serum albumin, pH ≈ 7, Biowest) as markers for medium-molecular-weight toxins.

The adsorption capacity of the BEA, RHO, PAU, and Y zeolites was measured spectrophotometrically. Zeolite samples weighing 20–25 mg were added to 20 mL of oxytocin, lysozyme, or albumin in a synthetic biofluid [16] that simulated a multicomponent physiological environment. This solution was treated under stirring for 20 h until an adsorption equilibrium was reached. The

Table 2. Main characteristics of marker proteins

Marker	Functionality	M_R, Da	Diameter, nm	Protein content
Oxytocin	Peptide hormone	1007 [13]	0.1	10 IU/mL
Chicken egg lysozyme	Enzyme	14300 [14]	3.5	95%
Bovine serum albumin (BSA)	Transport protein	66500 [15]	7.1	100%

samples were then centrifuged three times, and, using a Shimadzu UV-2600/2700 spectrophotometer (Shimadzu Europa GmbH), the optical density was measured at wavelengths corresponding to the maximum absorbance for the specific marker (i.e., oxytocin, lysozyme, or albumin). The concentration was derived from this optical density using a respective calibration curve. The maximum absorbance corresponded to wavelengths of 231 nm for oxytocin, 278 nm for albumin, and 272 nm for lysozyme.

The adsorption capacity was calculated by the formula:

$$q = \frac{(C_0 - C_t)V}{m},$$

where C_0 is the initial concentration of the tested protein in the solution (mg/L); C_t is the equilibrium concentration of the tested protein in the solution (mg/L); V is the solution volume (L); and m is the sample weight (g).

The hemolytic activity[1] of the synthetic zeolites was assessed for human erythrocytes using a hemolysis test [17]. See our previous studies [18] for a detailed description of this examination method. The zeolite content in the samples ranged from 0.3 to 10 mg/mL. The hemolytic activity was evaluated as a percent of the reference value, based on three independent experiments with three parallel samples being taken in each experiment. The amount of hemoglobin released from the destroyed erythrocytes was determined from the optical density measurements. The resultant statistics are illustrated in Fig. 4.

The cytotoxic effects of the tested synthetic zeolites on eukaryotic cells were evaluated using an MTT assay[2]. The adhesive culture of human endothelial cells, Ea.hy926, was used in the experiments. The solution prepared in plate cells was analyzed by evaluating the fluorescence intensity, a parameter measured on a Gemini EM plate reader (Molecular Devices, USA) at a wavelength of 590 nm with excitation at 560 nm at 37°C. Experimental data were collected using the Molecular Devices SoftMax Pro 5.2 software package. Three or four independent experiments were carried out, two experimental and two reference samples in each. The percentage of viable eukaryotic cells at zeolite concentrations of 2.5, 5.0, and 10 mg/mL was derived from the fluorescence intensity measured.

RESULTS AND DISCUSSION

The XRD patterns (Figs. 1a–1d) clearly show reflections typical of BEA, RHO, PAU, and Y zeolites, respectively, as well as the high purity and crystallinity of the zeolite samples prepared.

The SEM images were used to identify the sizes and morphology of the zeolite samples (Fig. 2).

All the zeolites were spherical in shape and had a fairly uniform size distribution of crystals (Figs. 2a–2d). The BEA, RHO, and PAU had a grain size of 200–300 nm. Figure 2d clearly shows the Y zeolite as 400–900 nm spheres with distinct crystalline outlines that consisted of aggregated disordered nanoparticles.

Figure 3 provides the low-temperature nitrogen adsorption/desorption isotherms of the BEA, RHO, PAU, and Y samples. Their porous properties are presented in Table 3.

Table 3 presents the specific surface area and the CEC determined by ion exchange with a hexamine cobalt solution.

The N_2 adsorption isotherms of the PAU sample are IUPAC type I, typical of microporous materials. The isotherms of BEA, RHO, and Y, with their hysteresis loops, are attributed to type IV and indicate the presence

[1] The hemolytic activity is the ability to induce hemolysis, i.e. to destroy red blood cells, leading to the release of hemoglobin into the cell environment.

[2] MTT assay is a colorimetric assay for assessing cell metabolic activity.

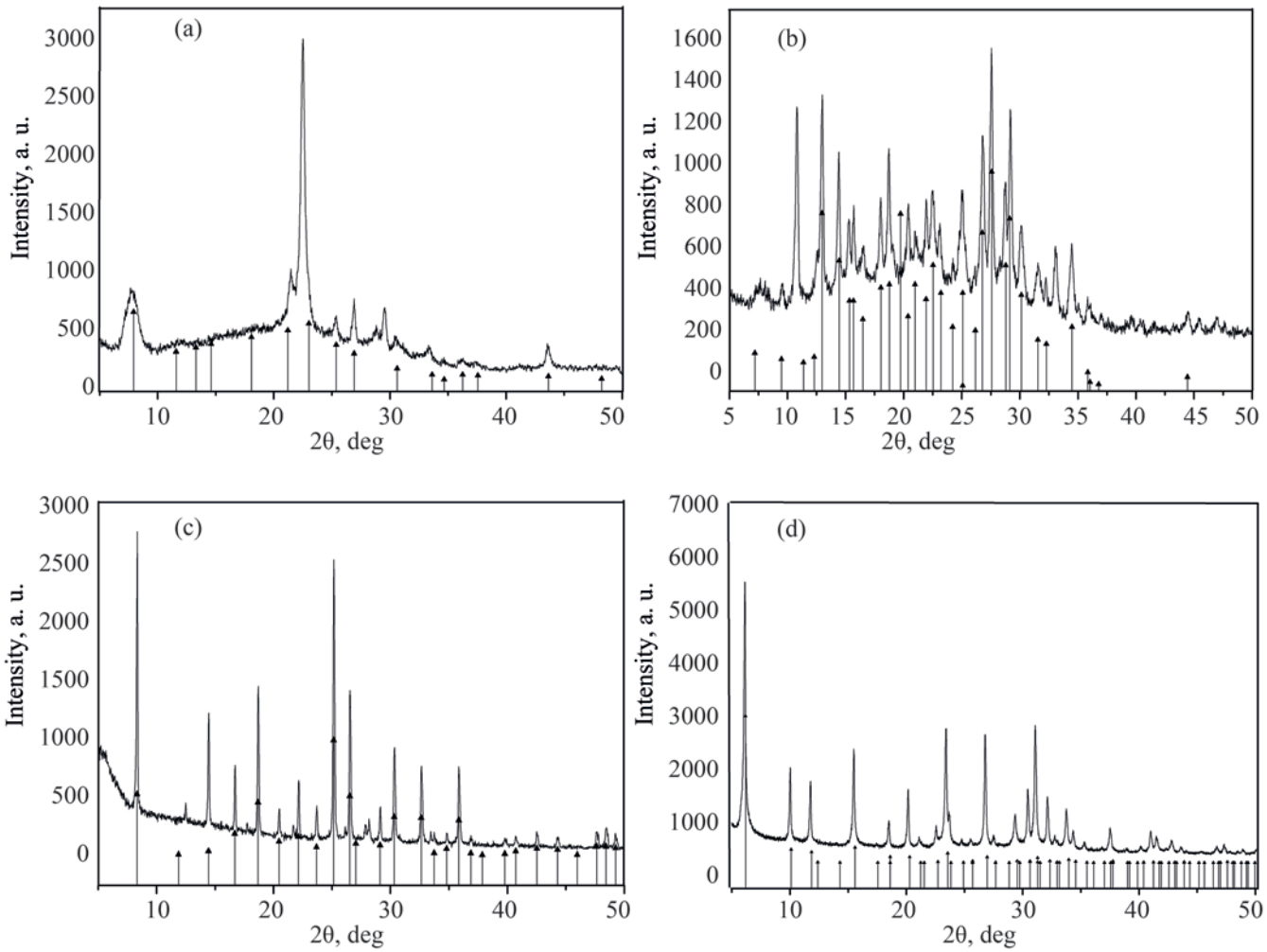

Fig. 1. XRD patterns: (a) BEA; (b) PAU; (c) RHO; and (d) Y. (▲) Line diagrams of BEA, PAU, RHO, and Y references, respectively.

of both micropores and mesopores (Fig. 3d). The RHO isotherm (Fig. 3b) shows only an adsorption curve above P/P_0 = 0.35 because over this range it intersects with the desorption curve. Given the microporosity of the zeolites, it was physically meaningless to evaluate the specific surface area (S) or pore size distribution for these samples. Nonetheless, for the purpose of rough estimation and comparative assessment of the samples under study, these parameters were determined (see Table 3).

The specific surface areas of the samples indicated in Table 3 were calculated using the Langmuir model, i.e. with due account of the contribution of micropores. The total pore volume was derived from the adsorption capacity at a near-saturation point. PAU is an ultra-

Table 3. Specific surface area, porosity, and CEC of zeolite samples

Sample	BEA	Y	RHO	PAU
S, m^2/g	892	569	967	–
S_{ext}, m^2/g	373	98	42	151
V_{pore}, cm^3/g	0.317	0.202	0.344	–
CEC, mg EQ/100 g	12±1	6±1	6.1±0.3	3.0±0.5

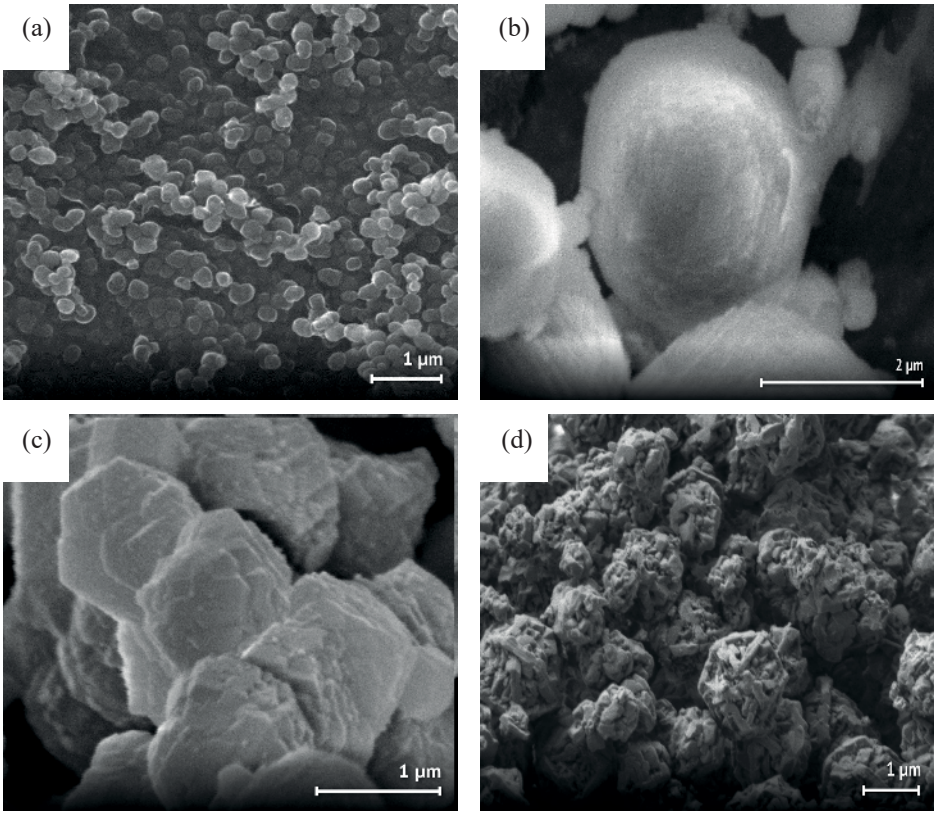

Fig. 2. SEM micrographs: (a) BEA; (b) PAU; (c) RHO; and (d) Y.

microporous material [19]. Bearing in mind its theoretical pore size (0.360 nm) and the nitrogen molecule size (0.364 nm), it is fair to state that low-temperature nitrogen adsorption is inapplicable for measuring the porous properties of this zeolite type. For PAU, therefore, only the external surface area (S_{ext}) can be used.

Table 4 presents the adsorption capacity of the studied zeolites for oxytocin, lysozyme, and albumin. Given that adsorption occurs on zeolite surfaces, it was important to find a correlation between the specific surface area and the adsorption capacity per 1 m^2 of the surface. Knowing that the sizes of the proteins exceeded those of the zeolite pore openings, it was safe to assume that the adsorption occurred on the external surfaces.

The data obtained suggest that the Y and BEA zeolites are exceptional for their high adsorption capacity. The BEA exhibited high adsorption capacity for all the model proteins: 50.0 mg/g for albumin, 48.3 mg/g for

Table 4. Adsorption capacity of zeolite samples

Sample	Adsorption capacity (q)					
	oxytocin		lysozyme		albumin	
	mg/g	μg/m^2	mg/g	μg/m^2	mg/g	μg/m^2
H-BEA	50.9±4.2	136.5	48.3±3.1	129.4	50.0±6.0	134.0
H-Y	50.5±0.4	515.3	20.7±0.4	211.2	0	0
H-RHO	26.4±2.4	628.6	20,2±0,2	481.0	0	0
H-PAU	19±0.9	125.8	28.5±0.1	188.7	0	0

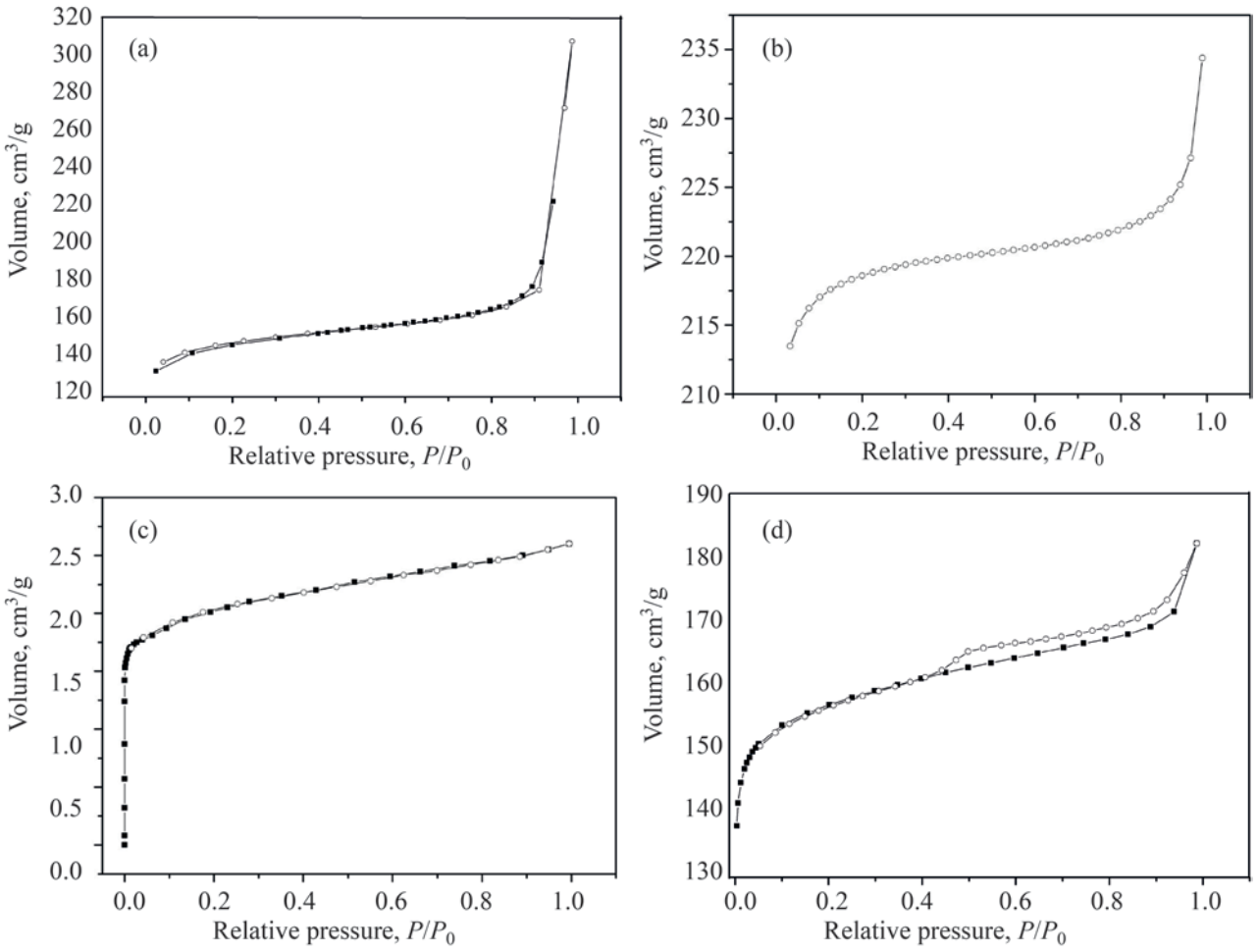

Fig. 3. Low-temperature nitrogen adsorption/desorption isotherms: (a) BEA; (b) PAU; (c) RHO; and (d) Y.

lysozyme, and 50.9 mg/g for oxytocin. This indicates a lack of selectivity in this zeolite type. In contrast, the Y zeolite proved to be selective towards low-molecular-weight proteins. Despite its relatively high adsorption capacity for oxytocin and lysozyme (50.5 and 20.7 mg/g, respectively), this sample did not adsorb the larger albumin molecules. On the other hand, the RHO and Y were superior in adsorption capacity for oxytocin and lysozyme per 1 m^2 surface, although the BEA's external surface area noticeably exceeded that of the RHO and Y. It is further worth noting that larger protein molecules corresponded to lower adsorption capacity of the zeolites, thus confirming that adsorption occurred on the external surfaces. The difference in the adsorptive properties of BEA and Y can be explained by their different porosity and texture. The larger values of external surface area, primary and secondary porosity, and CEC were likely responsible for the BEA ability to adsorb molecules with various molecular weights. The ultra-microporosity of RHO and PAU suggests that protein molecules adsorbed only on the external surfaces of these zeolites. Thus, it was demonstrated that the adsorption of proteins on the zeolites primarily depended on the external surface area.

The hemolytic activity of the tested samples for human erythrocytes is illustrated in Fig. 4.

These curves clearly show that, even at concentrations as low as 0.6 mg/mL, the RHO and PAU exhibited pronounced hemolytic activity (5.1 and 10.1%, respectively), and that the maximum hemolysis for these zeolites amounted to 37.9 and 40.7%, respectively. The BEA's hemolytic activity was negligible until its content reached 2.5 mg/mL. The hemolysis of the Y zeolite did not reach above 6% over the entire range of its content in the suspension (0.3–10 mg/mL).

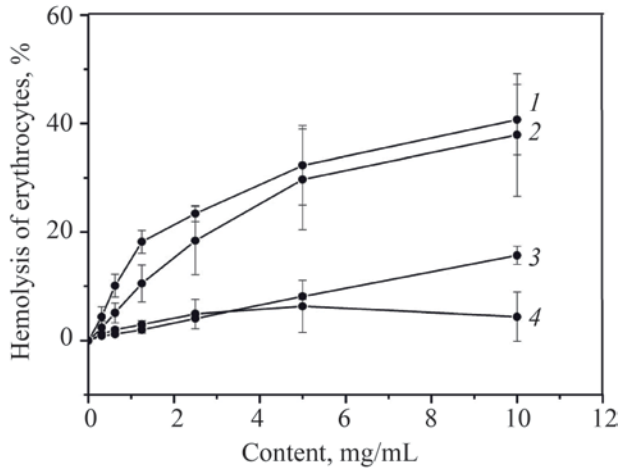

Fig. 4. Hemolytic activity of zeolite samples for human erythrocytes: (*1*) PAU; (*2*) RHO; (*3*) BEA; and (*4*) Y.

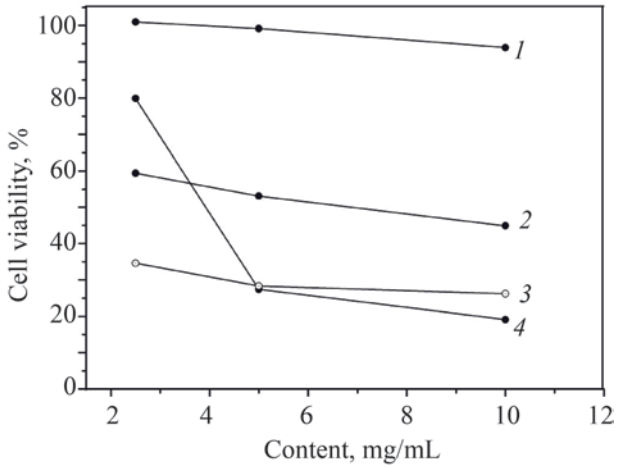

Fig. 5. Cytotoxicity of zeolite samples against human endothelial Ea.hy926 cells: (*1*) Y; (*2*) RHO; (*3*) PAU; and (*4*) BEA.

In general, the cytotoxicity assay results correlate with the hemolytic activity (Fig. 5). Special attention should be drawn to the Y zeolite: the Ea.hy926 cell viability remained high (almost 100%) over the zeolite content range of 0.3–10 mg/mL. In the presence of BEA, the cell viability was 80% even at 2.5 mg/g, not to mention its abrupt drop to 27% at 5 mg/g. The RHO and PAU exhibited similar cytotoxicity: over the entire range of 0.3–10 mg/mL, they significantly inhibited the growth of human Ea.hy926 cells (Fig. 5). It is reasonable to assume that RHO and PAU are unfeasible as medical sorbents.

The low cytotoxicity of the Y sample can be explained by the fact that it was synthesized in the absence of organic structure-directing agents (toxic templates). Following the same reasoning, the addition of organic templates (crown ether and TEAOH) during the synthesis of the RHO and PAU, respectively, was critical to the high toxicity of these zeolites. Although the organic template was removed by calcination to prepare the decationated zeolites, its residues may still have been present.

The high cytotoxicity of the RHO and PAU may also be caused by their large grain size (2–3 μm compared to 200–300 nm in the BEA). Therefore, although TEAOH was likewise added as an organic template to synthesize the BEA, its toxicity was markedly lower than that of the RHO and PAU. This assumption corroborates well with our prior studies [18].

Summarizing the data obtained, we clearly see a correlation between the grain size and cytotoxicity of the zeolites at low concentrations. Importantly, this correlation only makes sense for the zeolites synthesized with the addition of organic templates, specifically BEA, RHO, and PAU. Their cytotoxicity increases with the grain size in the following order: BEA < RHO < PAU. It is fair to posit that Ea.hy926 cells, capable of capturing microparticles, absorb zeolites, and this disturbs the metabolic activity of these cells. This capability also explains the higher cytotoxicity of the BEA at higher concentrations. Given that among all the tested zeolites, BEA had the smallest grain size (about 300 nm), a larger number of its particles can contact the cell, thus logically increasing its toxic effect compared to the other zeolites.

CONCLUSIONS

The hemolysis and cytotoxicity assay data suggest that Y and BEA are the least toxic of the zeolites under study. However, the BEA exhibited no pronounced cytotoxicity against blood erythrocytes or Ea.hy926 cells until its concentration exceeded 2.5 mg/g; in contrast, the Y zeolite proved to be low-toxic over the entire concentration range of 0.3 to 10 mg/mL. The BEA zeolite was distinguished by a well-developed specific surface area, a significant micropore volume, and high adsorption capacity for low- and medium-molecular-weight model toxins. The data strongly suggest that the Y zeolite would

be totally safe for humans and selective: it demonstrated an ability to effectively adsorb only low-molecular-weight proteins. These two zeolite types are very likely applicable as medical sorbents. Given their simultaneous high adsorption activity for protein components of a synthetic biofluid, these zeolites are promising sorbents for separation of biomolecules in affinity chromatography.

AUTHOR INFORMATION

N.Yu. Ul'yanova, https://orcid.org/0009-0004-3674-6207

E.Yu. Brazovskaya, https://orcid.org/0000-0001-6516-0417

O.Yu. Golubeva, https://orcid.org/0000-0002-4042-0718

O.V. Shamova, https://orcid.org/0000-0002-5168-2801

FUNDING

This study was carried out within the State Program of ISC RAS (project no. 0081-2022-0001).

CONFLICT OF INTEREST

The authors declare no conflict of interest requiring disclosure in this article.

REFERENCES

1. Ronco, C. and Bellomo, R., *Crit. Care*, 2022, vol. 26, no. 135, pp. 1–12. https://doi.org/10.1186/s13054-022-04009-w
2. Laurino, C. and Palmieri, B., *Nutricion Hospitalaria*, 2015, vol. 32, no. 2, pp. 573–581. https://doi.org/10.3305/nh.2015.32.2.8914
3. Clark W., R., Ferrari, F., La Manna, G., and Ronco, C., *Contribut. Nephrol*., 2017, pp. 43–57. https://doi.org/10.1159/000468911
4. Panichev, A.M., Bogomolov, N.I., Bogatova, N.P., Silkin, S.N., and Gulkov, A.N., *Zeolites in Surgery*, Vladivostok: FESTU, 2004, p. 120.
5. Souza, G., Villén, I., Viseras, F., and Perger Sibele, C., *Pharmaceutics*, 2023, no. 15(1352), pp. 1–33. https://doi.org/10.3390/pharmaceutics15051352
6. Norouzian, M.A., Valizadeh, R., Khadem, A.A., Afzal-zadeh, A., and Nabipour, A., *Biol. Trace Element Res*., 2010, vol. 137, no. 2, pp. 168–176. https://doi.org/10.1007/S12011-009-8574-8
7. Tomeckova, V., Rehakova, M., Mojzisova, G., Wadsten, T., Zelenakova, K., and Komanicky, V., *Spectroscop. Lett*., 2015, vol. 49, no. 2, pp. 63–72. https://doi.org/10.18097/PBMC20226803201
8. Amorim, R., Vilaca, N., Martinho, O., Reis, R.M., Sardo, M., Rocha, J., Fonseca, A.M., Baltazar, F., and Neves, I.C., *J. Phys. Chem. C*, 2012, vol. 116, no. 48, pp. 25642–25650. https://doi.org/10.1021/jp3093868
9. Berry, T.A., Belluso, E., Vigliaturo, R., Gieré, R., Emmett, E.A., Testa, J.R., Steinhorn, G., and Wallis, S.L., *Int. J. Environ. Res. Publ. Health*, 2022, vol. 19, no. 4031, pp. 1–17. https://doi.org/10.3390/ijerph19074031
10. Zhang, H., Kim, Ya., and Dutta, P.K., *Micropor. Mesopor. Mater*., 2006, vol. 88, nos. 1–3, pp. 312–318. https://doi.org/10.1016/J.MICROMESO.2005.09.026
11. Tang, T., Zhang, L., Dong, H., Fang, Z., Yu, Q., and Tang, T., *RSC Adv*., 2017, vol. 7, pp. 7711–7717. https://doi.org/10.1039/C6RA27129D
12. Golubeva, O.Yu. and Ul'yanova, N.Yu., *Glass Phys. Chem*., 2015, vol. 41, no. 5, pp. 537–544. https://doi.org/10.1134/S1087659615050065
13. Peters, T., *Adv. Protein Chem*., 1985, vol. 37, pp. 161–245. https://doi.org/10.1016/s0065-3233(08)60065-0
14. Ganz, T., *Encycloped. Respirat. Med*., 2006, pp. 649–653. https://doi.org/10.1016/b0-12-370879-6/00228-3
15. Henschen, A., Hupe, K.-P., Lottspeich, F., and Voelter, W., *The Quarterly Rev. Biol*., 1986, vol. 61, no. 4, pp. 532–536. https://doi.org/10.1086/415159
16. Tas, A.C., *Biomaterial*., 2000, vol. 21, no. 14, pp. 1429–1438. https://doi.org/ 10.1016/S0142-9612(00)00019-3
17. *Antibacterial Peptide Protocols*, Shafer, W.M., Ed., Humana Press., 1997, vol. 78, pp. 255–257.
18. Ulyanova, N.Yu., Kurylenko, L.N., Shamova, O.V., Orlov, D.S., and Golubeva, O.Yu., *Glass Phys. Chem*., 2020, vol. 46, pp. 155–161. https://doi.org/10.1134/S108765962002011X
19. Golubeva, O., Ulyanova, N., Yakovlev, A.V., *Glass Phys. Chem*., 2015, vol. 41, pp. 413–416. https://doi.org/10.1134/S1087659615040069